ISSN 0010-5082, Combustion, Explosion, and Shock Waves, 2022, Vol. 58, No. 2, pp. 135–148. © Pleiades Publishing, Ltd., 2022.
Russian Text © L. Pang, Q.-R. Hu, K. Yang.

Effect of Multiple Vent Parameters on an External Explosion Induced by an Indoor Premixed Methane–Air Explosion

L. Pang[a,b], Q.-R. Hu[a], and K. Yang[a,b,*]

UDC 536.46:614.841

Published in *Fizika Goreniya i Vzryva*, Vol. 58, No. 2, pp. 12–27, March–April, 2022.
Original article submitted March 22, 2021; accepted for publication June 9, 2021.

Abstract: To reveal the influence of vent parameters on the dynamic mechanism of an external explosion induced by a vented premixed methane–air explosion, the evolution process of an outdoor flow field under different vent opening pressures (p_v), opening times (t_v), and scaled vent size ($K_v = A_v/V^{2/3}$) is studied by methods of computational fluid dynamics. With an increase in K_v, the shape of the unburned gas cloud and vented flame gradually changes from a jet shape to a depression toward the vent. The outdoor peak specific turbulent kinetic energy increases by 36.5 and 4 times with an increase in p_v and t_v, respectively. At $t_v = 0.1$ s, the peak specific turbulent kinetic energy reaches 1411 m^2/s^2 and the turbulence range reaches 3 times the length of the room. With an increase in p_v, t_v, and K_v, the occurrence time interval of the external explosion exhibits a decreasing trend. The external explosion is located at a distance of less than 1.4 times the length of the room. At $K_v = 0.05$, the external explosion occurs at the furthest location.

Keywords: gas explosion, vented explosion, external explosion, flow field, venting hazard.

DOI: 10.1134/S0010508222020022

INTRODUCTION

Explosion venting is an effective method for controlling the hazard of a gas explosion occurring in a confined space [1]. As the high-pressure unburned gas and combustion products are promptly released to the outdoors during explosion venting, the indoor explosion peak overpressure rapidly decreases, allowing the damage to equipment and the building due to the explosion overpressure to be limited [2]. However, if a vented explosion occurs in a confined space, a large amount of a combustible gas and a high-speed flame are discharged through the vent at the instant of its opening, causing complex changes in the outdoor flow field. Under certain special conditions, the vented flame can ignite the outdoor flammable gas cloud, and an external explosion can occur, potentially inducing a serious secondary disaster and posing a potential threat to the surrounding environment, equipment, and personnel [3, 4].

The gas explosion mechanism and the hazard effect of explosion venting have always been the focus of scientists. Moen et al. [5] used a 50-m^3 circular pipe to study the effects of the area blocking rate and orifice blockage on the explosion venting of a methane–air mixture. Diakow et al. [6] found that relatively small repeated congestion can significantly increase the explosion overpressure in the pipeline. McCann et al. [7] used small-scale experimental devices with windows on both sides to conduct gas explosion venting studies. They observed the dynamic behaviour of earlier vented flame development and discovered the trigger mechanism of pressure oscillations. Subsequently, Cooper et al. [8] conducted a vented explosion experiment in a cubic vessel with a side length of 0.91 m and observed a four-peak structure in the explosion overpressure curve; the conclusion laid the foundation for research on the explosion venting overpressure structure formation mechanism. The peak overpressure caused by external explosions is a

[a]School of Safety Engineering, Beijing Institute of Petrochemical Technology, Beijing, 102617 China; *ycyangk@bipt.edu.cn.
[b]Beijing Academy of Safety Engineering and Technology, Beijing, 102617 China.

significant feature of the indoor explosion pressure [9]. Chao et al. [10] and Bauwens et al. [11] proposed a venting overpressure structure calculation method based on the principles of previously reported simplified analysis models [12–15]. The peak external explosion overpressure has attracted the attention of many scholars. At present, a large number of scientists have studied the effects of the ignition position [16], gas concentration [17], equivalence ratio [18], opening pressure [19], vent size [20], opening time [21], inertia [22], and initial turbulence [23] on the characteristics of the external explosion overpressure induced by indoor gas explosions. The outdoor flow field is extremely complicated because of vented explosions [24–27]; as a result, the process of an external explosion induced by a vented gas explosion is extremely complicated, involving various physical processes such as combustion, thermodynamics, and fluid dynamics. The results demonstrated that a high-speed combustible gas was ejected through the vent due to an indoor and outdoor pressure difference, and a combustible gas cloud was formed outdoors [28]. When the vented flame reached the outside, the external high-temperature preheated gas cloud was ignited and severe turbulent combustion occurred, which led to a sharp increase in the outdoor pressure [29]. Relevant research has demonstrated that the occurrence of an external explosion requires three conditions [30]: (1) large amount of the combustible gas; (2) severe turbulence and vortices; (3) vented flame. These conditions are significantly affected by the vent parameters, but only few studies have been focused on this aspect. Researchers often concentrate on the external explosion overpressure, without a systematic analysis of the outdoor flow field and external explosion characteristics under different vent conditions. Hence, it is not conducive to propose the hazard control and mitigation measures from the perspective of the evolution process of external gas explosions.

Therefore, this study used the computational fluid dynamics (CFD) technology to establish a physical model of a large-scale explosion. A vented methane–air mixture explosion was used as a research object. The temporal and spatial evolution of the external unburned gas cloud, vented flame, and turbulence for different opening pressures, opening times, and scaled vent sizes was explored, and the distribution differences of the external explosion overpressure, explosion occurrence time, and location were summarised and analysed. The research results have important theoretical and practical significance for establishing accurate external explosion overpressure prediction models, scientifically designing explosion pressure relief facilities, and mitigating the hazardous effects of external explosions.

1. RESEARCH METHODS

AutoReaGas based on the CFD technology is a three-dimensional commercial software for computational fluid analysis, a finite-volume computational code for fluid dynamics suitable for gas explosion problems [31]. Its reliability has been verified in the famous BFETS and MERGE experimental tests, the numerical simulation and experimental results were in good agreement, and a large number of scholars have successfully used the code [32, 33]. Therefore, the software was used to research explosions of a premixed gas in confined spaces in this study.

1.1. Governing Equations

The gas explosion solver in AutoReaGas (Version 3.1) uses the finite volume method to solve the mass, momentum, and energy conservation equations [34]. The combustion reaction is regarded as a one-step conversion process from the reactant to the product. The calculation method for the volumetric combustion rate R_c in the mass conservation equation was proposed by Salzano et al. [35]:

$$R_c = C_t \rho \frac{S_t^2}{\Gamma} \min[m_{\text{fuel}}, m_{\text{O}_2}, m_{\text{pr}}]. \tag{1}$$

Here C_t is a dimensionless constant, which represents the main adjustable parameter and was set according to the previous sensitivity analyses, ρ is the mixture density, S_t is the turbulent combustion speed, Γ is the turbulent diffusion coefficient for mass and/or energy, m_{fuel} is the fuel mass fraction, m_{O_2} is the oxygen mass fraction, and m_{pr} is the mass fraction of combustion products.

Turbulence is a key factor in the gas explosion mechanism. The k–ε model is used for modelling, which contains the conservation equation of the turbulent kinetic energy k and its dissipation rate ε [36]:

$$\frac{\partial}{\partial t}(\rho k) + \frac{\partial}{\partial x_j}(\rho u_j k) = \frac{\partial}{\partial x_j}\left(\Gamma_k \frac{\partial k}{\partial x_j}\right) + \tau_{ij}\frac{\partial u_i}{\partial x_j} - \rho\varepsilon, \tag{2}$$

$$\frac{\partial}{\partial t}(\rho \varepsilon) + \frac{\partial}{\partial x_j}(\rho u_j \varepsilon) = \frac{\partial}{\partial x_j}\left(\Gamma_\varepsilon \frac{\partial \varepsilon}{\partial x_j}\right) + C_1 \frac{\varepsilon}{k}\tau_{ij}\frac{\partial u_i}{\partial x_j} - C_2 \frac{\rho \varepsilon^2}{k}, \tag{3}$$

where C_1 and C_2 are constants, and τ_{ij} is the viscous stress tensor expressed as

$$\tau_{ij} = \mu_t\left(\frac{\partial u_i}{\partial x_j} + \frac{\partial u_j}{\partial x_i}\right) - \frac{2}{3}\delta_{ij}\left(\rho k + \mu_t \frac{\partial u_i}{\partial x_j}\right), \tag{4}$$

Table 1. Set of constants used in the AutoReaGas code

Constant	Value
Combustion speed:	
laminar combustion F_s	0.15 [Eq. (6)]
turbulent combustionC_t	40 [Eq. (1)]
k–ε Model:	
C_μ	0.09
C_1	1.44
C_2	1.79
σ_k	1.0
σ_ε	1.3
F_k	0.5

where δ_{ij} is the Kronecker delta, and μ_t is the turbulent viscosity.

Bray [37] conducted a correlation analysis on a large number of experimental data of turbulent flame propagation and derived the relationship between the turbulent combustion speed S_t and turbulence

$$S_t = 1.8 u_t^{0.412} L_t^{0.196} S_l^{0.784} \nu^{-0.196}, \tag{5}$$

where $u_t = \sqrt{(2/3)k}$ is the turbulence intensity, $L_t = C_\mu^{0.75}(k^{3/2}/\varepsilon)$ is the turbulence characteristic length scale, C_μ is the model constant, S_l is the laminar combustion speed of the flammable mixture, and ν is the kinematic viscosity of the flammable mixture.

A quasi-laminar modification was used for the initial laminar combustion speed. The effects of pressure, temperature, and flame front wrinkling on the laminar combustion speed are described by a second adjustable parameter F_s, which relates $S_{l,\text{eff}}$ to the flame radius r and to the theoretical laminar flame speed [31]. In the current version of the AutoReaGas code, the laminar combustion speed increases in proportion to the spherical flame radius (r) as

$$S_{l,\text{eff}} = S_l(1 + F_s r), \tag{6}$$

where $S_{l,\text{eff}}$ is the effective laminar combustion speed, and F_s is the proportionality factor. The set of all constants used in the AutoReaGas code is shown in Table 1.

1.2. Numerical Models

The AutoReaGas code uses the finite volume method to solve the Navier–Stokes and Euler partial differential equations, and the computational domain is subdivided into a finite number of rectangular control bodies ΔV. The scalar function $\varphi(x, y, z, t)$ is defined at the centre of these rectangular control bodies. To ensure coupling between the velocity and pressure fields, the fluid velocity is defined at the centre of the control volume interface; thus, each momentum conservation equation must be solved in a control volume grid staggered relative to the position of the scalar control volume system.

The AutoReaGas code ensures a gradual transition from the "central" scheme of the diffuse dominant flow to the upwind scheme of the convective dominant flow. The SIMPLE method [34] extended for a compressible flow was used in computations. This method introduces a new variable (pressure correction), which makes the necessary corrections to the velocity components, pressure, and density to ensure that the mass conservation constraint is obeyed at a new time level. The pressure and density are corrected as necessary to obey the conservation of mass at a new level of time to achieve convergence.

In the current version, the first-order upwind time integration scheme and adaptive time step are used to solve for time, and stability of the solving algorithm is achieved by controlling the maximum time step and ensuring the Courant–Friedrichs–Lewy stability criterion

$$\Delta t = \frac{\omega \Delta x}{c + |\boldsymbol{v}_s|}, \tag{7}$$

where Δt is the maximum allowable time increment, ω is the time step safety factor equal to 1.0, Δx is the minimum spatial cell size, c is the sound velocity in the cell grid, and $\boldsymbol{v}_s$ is the velocity vector.

1.3. Verification of Grid Independence

The numerical software was used an 8-node structure grid to discretise the space, while using the sub-grid technology to describe the effect of small-scale entities on the flow field [32]. A 6 × 3 × 2.5 m room with no obstacles was selected to investigate the effect of the grid size on the accuracy when capturing the explosion flow field. A 0.5 × 0.5 m vent was set in one of the smaller walls of the room.

The room was filled with a static premixed methane–air gas at a volume concentration of 10%, and the ignition source was located at the geometric centre of the rear wall. Two cubic grids 0.1 × 0.1 × 0.1 m (M1) and 0.05 × 0.05 × 0.05 m (M2) were used to mesh physical models, and the peak overpressures of the two examples were compared and analysed. Table 2 lists the peak overpressures for the two grid sizes. It was concluded that the relative discrepancy in the peak overpressure was less than 3%, indicating that the grid size had a minor effect in this work, and both grids were suitable for this study [21]. Therefore, to save time and improve the calculation efficiency, the M1 grid was used to perform the numerical calculations in the following

Table 2. Comparison of peak overpressures

Distance to the back wall, m	$p_{e,\max}$, kPa		Discrepancy, %	
	380 091* (M1)	936 411* (M2)	absolute	relative
0.5	32.83	32.86	0.03	0.09
2.5	31.64	31.70	0.06	0.19
5.5	30.06	30.11	0.05	0.17
11.5	52.94	54.08	1.14	2.15
19.5	20.09	19.66	0.43	2.14

*Total number of nodes in the grid.

Table 3. Parameters used in the numerical model for validation

Parameter	Value
Laminar flame acceleration coefficient	0.15
Dimensionless constant	40
Initial ambient pressure	$1.01325 \cdot 10^5$ Pa
Initial ambient temperature	300 K
Turbulent kinetic energy	$1 \cdot 10^{-5}$ m^2/s^2
Turbulent kinetic energy dissipation rate	$1 \cdot 10^{-5}$
Turbulent kinetic energy conversion factor	1
Turbulence intensity	$2.58 \cdot 10^{-3}$

studies. To increase the accuracy of computations, the adaptive grid technology was used in some regions of the computational domain for automatic tuning of the grids.

1.4. Experimental Validation of the Numerical Model

To verify the applicability of the selected numerical model to this study, the results of the numerical simulation and large-scale methane–air explosion experiment of Tomlin et al. [27] were compared. The same parameters and conditions were used in this model verification as in the experiment, in which the methane volume concentration was 9.5%. The venting surface completely ruptured immediately after reaching its opening pressure. The outside air was static. All parameters used in the numerical model for validation are presented in Table 3. The experimental and computed overpressure curves are compared in Fig. 1.

The trend of the numerical and experimental overpressure curves was approximately the same, and the maximum relative discrepancy of the peak overpressure was 5.8% (see Fig. 1b). The peak p_{ac} related to the acoustics of the explosion chamber was not observed in the numerical results; this is because the numerical simulation usually assumes the wall of the chamber as a rigid wall and, thus, cannot predict the structural response of the explosion chamber, which hinders the interaction between the acoustic vibration and structural response [26]. The coupling effect makes it impossible to observe the peak p_{ac}, and this study mainly deals with the external explosion flow field; hence, this pressure peak is not considered.

It should be noted that the explosion overpressure was mainly studied, and thus this study did not further verify the mixture fraction and turbulence. However, the overpressure, mixture fraction, and turbulence are correlated in the governing equations, which have been widely approved [20].

2. RESEARCH PLANS

Based on the general characteristics of the gas explosion hazard in an ordinary room, a cuboid physical model with a size of 6 × 3 × 2.5 m (length × width × height) was used. The four walls of the room, as well as the roof and floor, were adiabatic smooth rigid surfaces. A square vent was arranged in one of the smaller walls and was able to completely break immediately after reaching the set opening pressure or opening

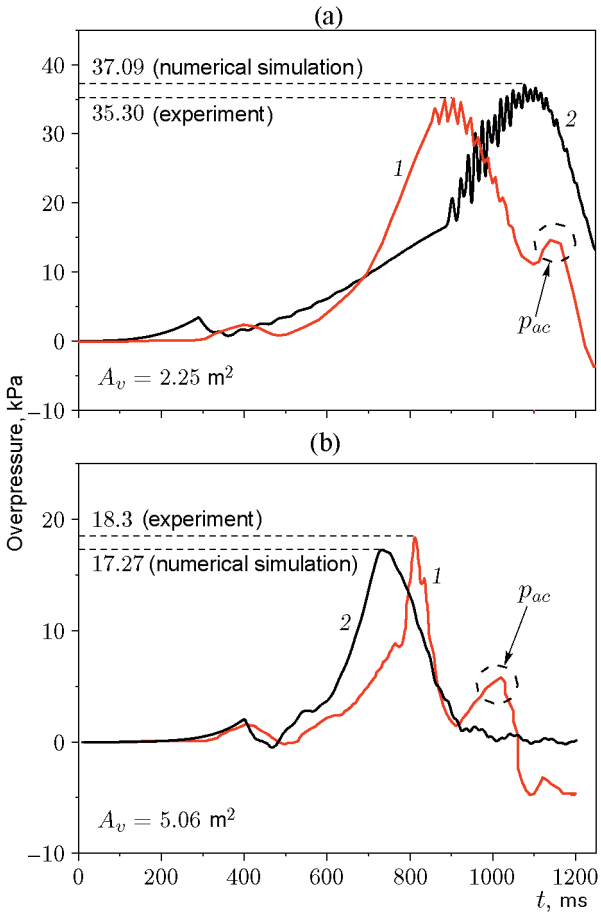

Fig. 1. Experimental (*1*) and numerical (*2*) overpressure curves for different vent sizes.

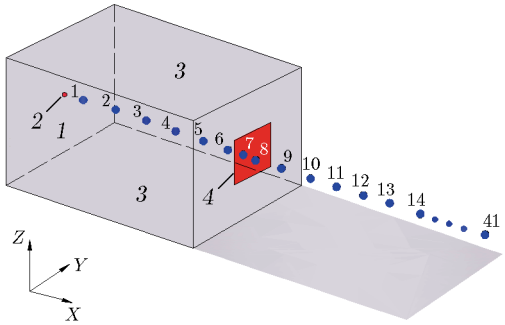

Fig. 2. Sketch of the room and arrangement of measuring points: (*1*) back wall; (*2*) ignition; (*3*) adiabatic solid wall; (*4*) vent; the gauges are numbered from 1 to 41.

time. According to the relevant literature [29], a volume concentration of 10% was considered to be the best concentration for a methane explosion. Thus, a static methane–air premixed mixture with a volume concentration of 10% was used in this study. Backwall ignition usually leads to a strong external explosion. Therefore, a spherical point ignition source with a radius of 0.015 m was set at the geometric centre of the back wall of the room at a distance of 0.1 m from the back wall. The influence of the ignition source on the explosion flow field was not considered. There were no obstacles in the room. To accurately capture the effect of the external explosion on the indoor overpressure, the calculation domain was extended to 5.5 times the length of the room in the direction of the vent, so that it had a size of $39 \times 3 \times 2.5$ m, and the extended calculation domain was set as the free outflow boundary. The outside air was in a static state, and the initial ambient pressure and temperature in the calculation domain were set to $1.01325 \cdot 10^2$ kPa and 300 K, respectively. All parameters in the model were set by default, as listed in Table 3. All the measuring points were located on the central axis of the room, with measuring point 1 located at 0.5 m from the back wall and measuring points 7 and 8 arranged at 0.1 m on both sides of the vent; the other measuring points were arranged at equal intervals of 1 m. A sketch of the room and arrangement of the measuring points are shown in Fig. 2.

In this study, the effects of the vent opening pressure (p_v), opening time (t_v), and scaled vent size ($K_v = A_v/V^{2/3}$, where A_v [m^2] is the vent area, and V [m^3] is the volume of the explosion chamber) on the mechanism of the external explosion induced by an indoor methane explosion were investigated. The vent opening pressures in this study were 20, 30, 40, and 50 kPa as the static opening pressure of civil building window glass is approximately 7–60 kPa. The vent opening times in this study were 0, 0.02, 0.06, and 0.1 s. Based on the range of the scaled vent size used in the related literature [20], a scaled vent size of 0.05–0.18 was used in this work.

3. RESULTS AND DISCUSSION

3.1. Effect of the Vent Parameters on the Outdoor Flow Field

3.1.1. Distribution of the Characteristics of the Unburned Gas Cloud. Figure 3 shows a nephogram of the mass concentration distributions of the unburned gas when external explosions occur under different vent parameters. Based on jet theory [33], the process of methane being discharged to the outdoors through the vent can usually be regarded as a variable density jet in an infinite static environment. It can be seen from

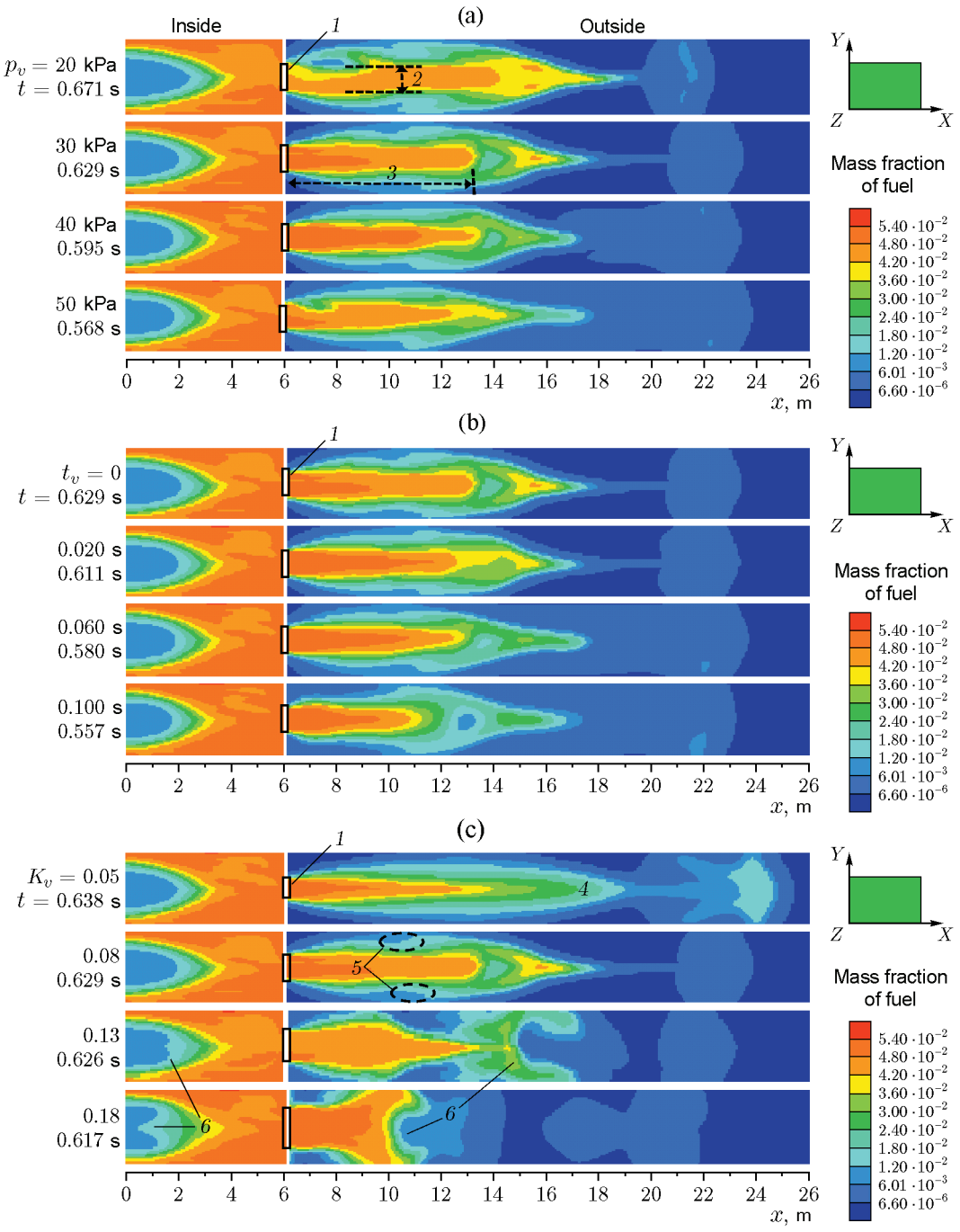

Fig. 3. Mass fraction of the unburned gas cloud for different vent parameters: (a) opening pressure ($t_v = 0$ and $K_v = 0.08$); (b) opening time ($p_v = 30$ kPa and $K_v = 0.08$); (c) scaled vent size ($p_v = 30$ kPa and $t_v = 0$); (*1*) vent; (*2*) radial width; (*3*) axial length; (*4*) jet shape; (*5*) folds; (*6*) sag.

Figs. 3a and 3b that the vent opening pressure and opening time have similar effects on the distribution of the characteristics of the outdoor unburned gas clouds. The external unburned gas cloud generally has a jet shape, and the gas cloud concentration gradually decreases radially from the centre line of the vent. The widths of the radial distributions of the high-concentration unburned gas clouds (>0.042) were the same, but, as the opening pressure and opening time decreased, the axial distribution length of the high-

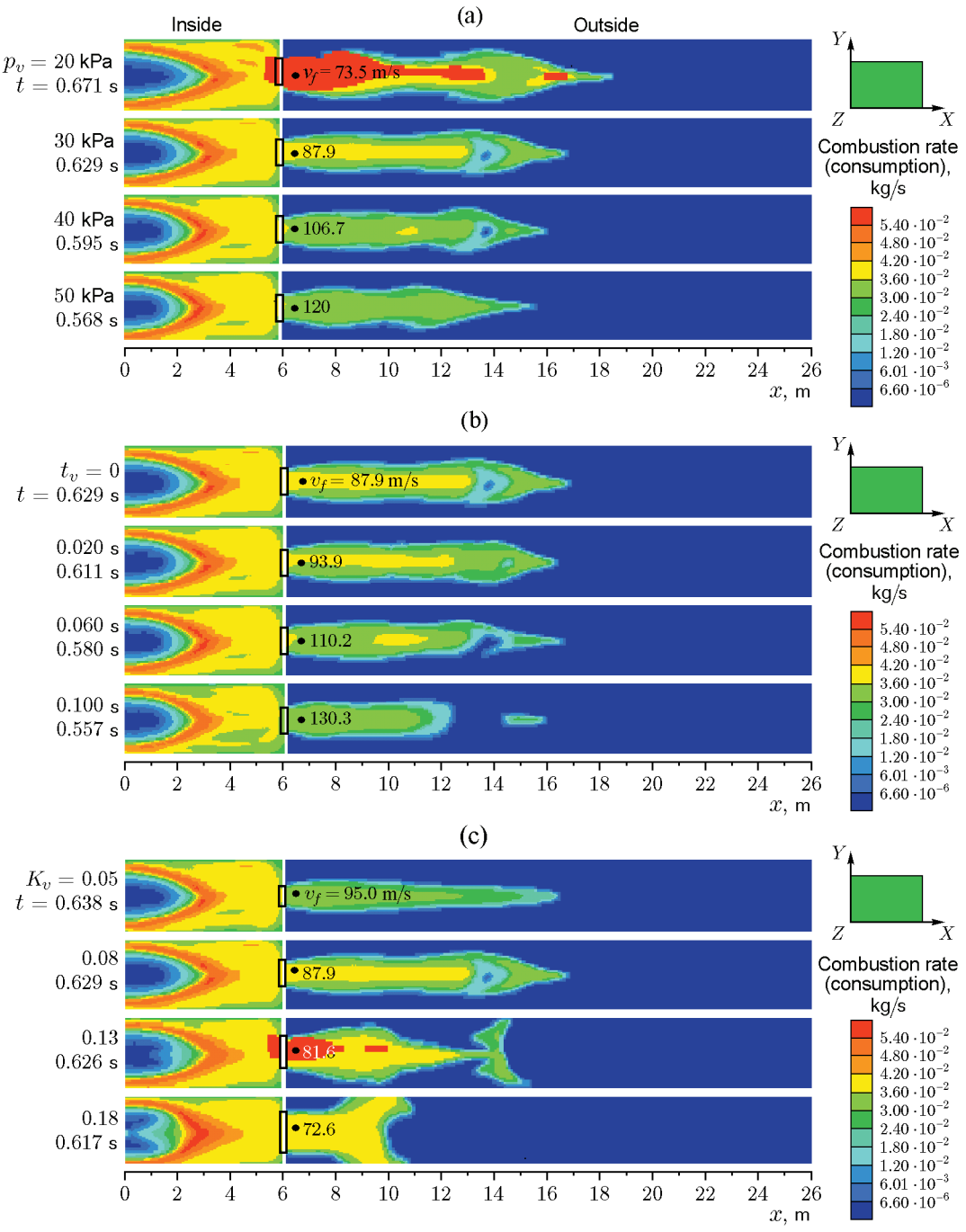

Fig. 4. Vented flame propagation nephogram for different vent parameters: (a) opening pressure (t_v = 0 and K_v = 0.08); (b) opening time (p_v = 30 kPa and K_v = 0.08); (c) scaled vent size (p_v = 30 kPa and t_v = 0).

concentration unburned gas cloud gradually increased. Simultaneously, it can be seen from Fig. 3c that the radial distribution width of the high-concentration gas cloud increased and the axial distribution length first increased and then decreased with an increase in the scaled vent size K_v. At K_v = 0.05, the shape of the unburned gas cloud was a wrinkle-free jet, and the edges were more regular. When methane is injected into a static ambient medium, there appear discontinuities. These discontinuities usually lose their stability

after they are subjected to the action of disturbances and generate a vortex, which entrains the ambient air into the jet, simultaneously moving and deforming the latter. The influence of the vortex is gradually extended to the indoor and outdoor sides, forming a mixed layer of free turbulence. At $K_v \geqslant 0.13$, the velocity of the escaping hot gas is lower than that at $K_v = 0.05$; therefore, the mixture is less turbulent, leading to gradual reduction of the axial distribution length of the unburned gas cloud. With an increase in K_v, the radial distribution width of the high-concentration gas significantly increases, and the shape of the vented gas cloud wrinkles and deforms; this is because the indoor and outdoor pressure difference decreases with an increase in the scaled vent size at the moment the vent ruptures, and the spreading speed of the vented unburned gas cloud also decreases. Then, the cloud edge becomes more sensitive to friction and to the fact that outdoor air prevents the cloud motion. As a result, the cloud gradually loses its stability. During unburned gas cloud expansion in static outdoor air, there appears a shear layer, leading to the Helmholtz instability.

3.1.2. Characteristicsof Vented Flame Propagation. Figure 4 shows the vented flame development for external explosions that occur at different vent characteristic parameters. A comparison between Figs. 3 and 4 shows that the shape of the vented flame is consistent with the distribution characteristics of the unburned gas cloud. At $K_v < 0.08$, the observed jet flame should be formed by continuous burning of the discharged high-concentration unburned gas mixture. As the vent opening pressure and opening time increase, the flame propagation distance and burning velocity of the external gas gradually decrease. As the scaled vent size increases, the flame propagation distance also gradually decreases, but, because of the lumped high-concentration unburned gas cloud, the burning velocity of the external gas gradually increases (>0.036 kg/s). In addition, the flame propagation speed mainly consists of the gas burning velocity and gas flow diffusion speed, with a higher outflow velocity of the vented gas leading to a greater flame propagation speed. Thus, as the opening pressure and opening time increase and the scaled vent size decreases, the flame propagation speed near the vent increases from 73.5 to 120.5 m/s, from 87.9 to 130.3 m/s, and from 72.6 to 95 m/s, i.e., the maximum rate of change reaches 64, 48, and 24%. It can be seen that the vent opening pressure and opening time have the most significant effects on the vented flame propagation speed; its maximum value can reach more than 100 m/s, which may cause a severe external explosion hazard effect.

3.1.3. Turbulence Intensityof the Outdoor Flow Field. As a measure of the turbulence intensity of the outdoor flow field, the specific turbulent kinetic energy can be used to characterise the turbulence degree of the flow field to some extent. Figure 5 shows the distributions of the peak specific turbulent kinetic energy in the axial direction of the centre line of the vent (x axis) for external explosions that occur at different vent parameters. As the range of the methane jet increases, more entrained air gains momentum and flows forward with the jet, while the momentum of the methane jet and its speed decrease. The entrainment of air by the jet leads to continuous expansion of the jet cross section, while the flow velocity continues to decrease, thereby reducing turbulence. It can be seen from Fig. 5 that all the external peak specific turbulent kinetic energy values in the axial direction first increase and then decrease. Meanwhile, the outdoor turbulence intensity significantly increases with the vented gas velocity, which is influenced by the opening pressure, opening time, and scaled vent size. Therefore, with an increase in the opening pressure and opening time, the maximum peak specific turbulent kinetic energy of the outdoor flow field increases from 28 to 1050 m^2/s^2 and from 279 to 1411 m^2/s^2, respectively, i.e., by 36.5 and 4 times. This means that the outdoor turbulence intensity is significantly affected by the vent parameters, and a larger turbulence intensity will make the outdoor explosion flow field more complicated.

Based on the turbulence theory for external gas flows, the flow state can usually be considered as turbulent if the Reynolds number (Re) is greater than $500 \cdot 10^3$. At $\mathrm{Re} = 500 \cdot 10^3$, the turbulence intensity I calculated by the formula

$$I = 0.16\mathrm{Re}^{-1/8} \tag{10}$$

is equal to 3.1%.

In the present study, the maximum velocity of the outdoor gas flow was greater than 30 m/s. The critical turbulent kinetic energy k determined by the formula

$$k = 3/2(UI)^2, \tag{11}$$

should be 1.3 m^2/s^2. Therefore, the turbulent area range is defined as $k \geqslant 1.3$ m^2/s^2. As shown in Figs. 5a and 5c, as p_v increases from 20 to 50 kPa and K_v decreases from 0.18 to 0.05, the turbulence area ranges increase from 5 to 17 m and from 8 to 16 m, respectively, and the maximum increase rates are all greater than 100%. However, the maximum increase rate of the turbulence area range (32.9%) is relatively low, as shown in Fig. 5b. Thus, the vent opening time seems to have a smaller effect on the turbulence area range.

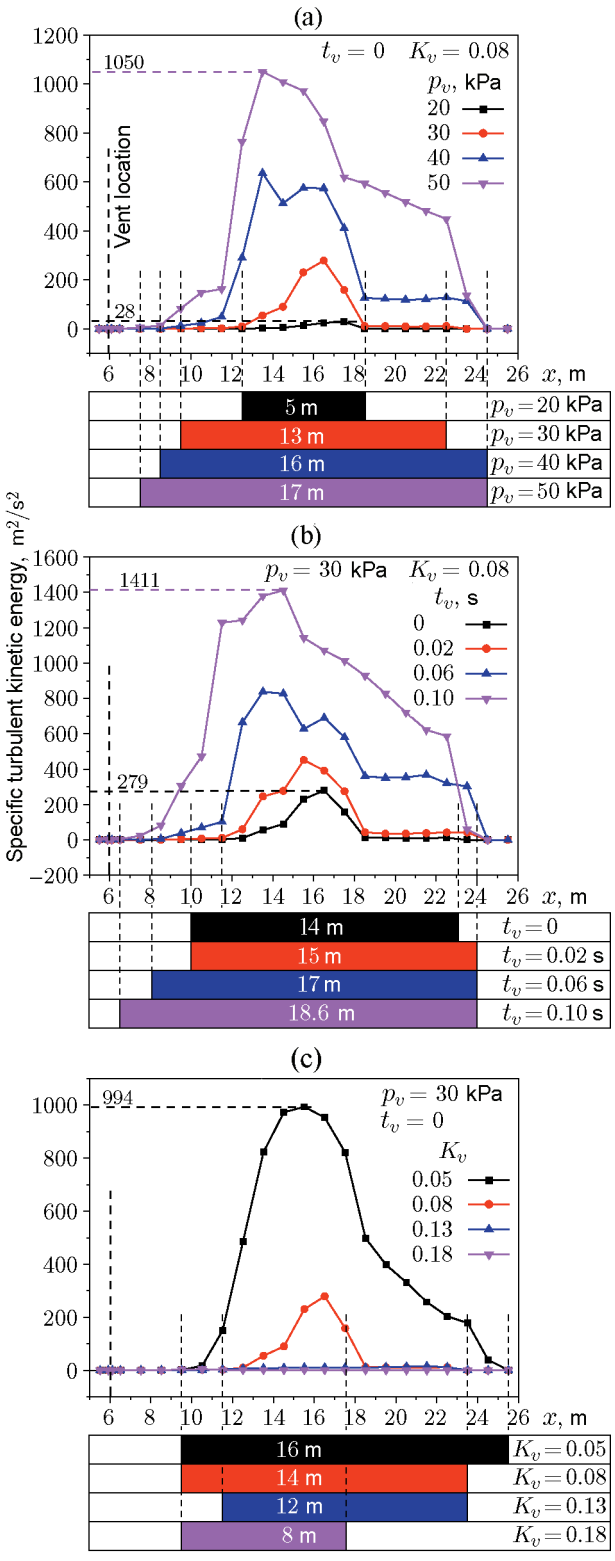

Fig. 5. Specific turbulent kinetic energy along the x axis for different vent parameters: opening pressure (a), opening time (b), and scaled vent size (c).

3.2. Effect of the Vent Parameters on the External Explosion

3.2.1. External Explosion Overpressure. The occurrence and intensity of an external explosion depend on matching and coupling of multiple factors. For example, the jet flame used for ignition should have sufficient turbulence intensity and vented propagation speed; the external unburned cloud should also have a suitable flow field structure. The above-mentioned factors are affected by many constraints, such as the opening pressure and scaled vent size, resulting in significant changes in the external explosion overpressure. The peak explosion overpressure is plotted against the distance for different vent parameters in Fig. 6. It can be seen that, because of the strong gas explosions outdoors, the outdoor peak overpressures p_e are higher than those of the indoor environment. Figure 6a shows that the maximum outdoor peak overpressure increases with the opening pressure from 42.89 to 73.75 kPa. Meanwhile, Fig. 6b shows that the maximum outdoor peak overpressure first increases and then decreases with an increase in the opening time. The peak overpressure reaches a maximum (p_e = 74.39 kPa) when the opening time is 0.06 s and then begins to decrease as the opening time continues to increase. The indoor gas burning time increases because of the increase in the opening time, which consumes a large amount of the combustible gas. Thus, the amount of the unburned gas discharged outdoors decreases. Finally, the concentration of the outdoor unburned gas cloud decreases, and the distribution length of the high-concentration unburned gas cloud decreases in the axial direction (see Fig. 3b). As K_v increases from 0.05 to 0.18, the maximum external peak overpressure first increases and then decreases (Fig. 6c). At K_v = 0.08, the external explosion peak overpressure reaches its maximum: p_e = 63.92 kPa). However, at $K_v > 0.08$, it can be seen from a comparison between Figs. 4c and 5c that the vented flame propagation speed decreases and the outdoor flow field turbulence weakens, causing the external explosion overpressure to decrease rapidly.

3.2.2. Time Interval of External Explosion Occurrence. In Fig. 7, the curves for the time interval between the instant when the vent opens and the external explosion occurs are plotted against different vent parameters. It is seen that the occurrence time Δt of the external explosion gradually decreases with an increase in the opening pressure, opening time, and scaled vent size. The decrease in time interval (Δt = 0.02 s) is the smallest one with an increase in K_v, and its maximum relative reduction rate is only 8%. However, the decrease in the time interval is greater than 0.07 s as the

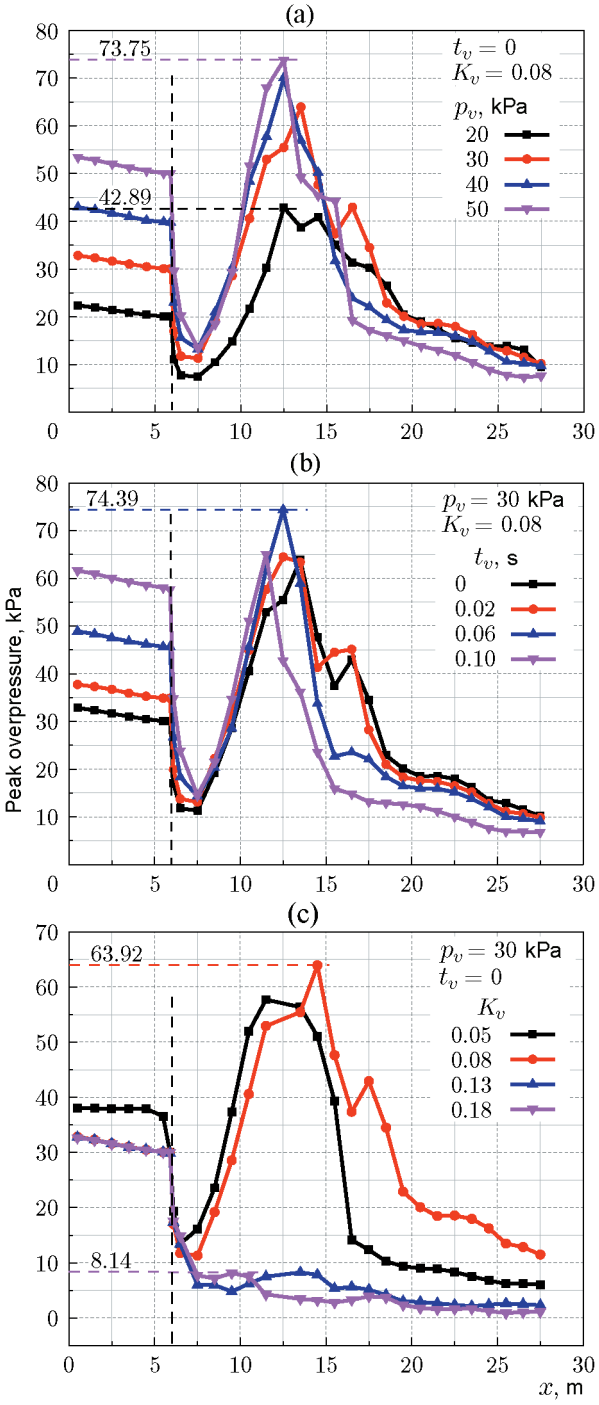

Fig. 6. Peak overpressure versus the distance for different vent parameters: opening pressure (a), opening time (b), and scaled vent size (c).

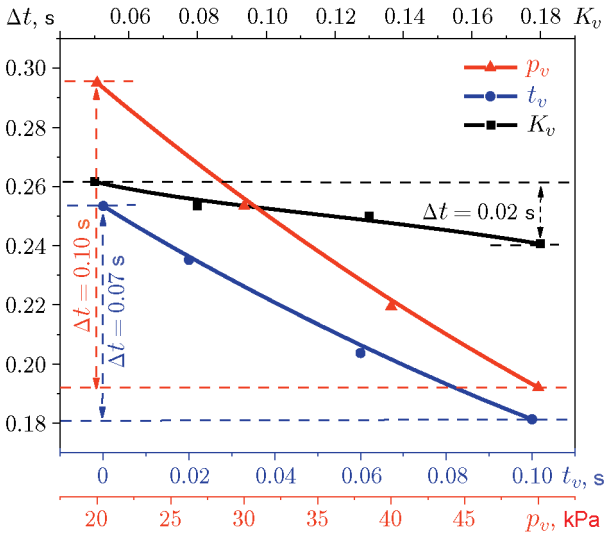

Fig. 7. Time interval of external explosion occurrence for different vent parameters.

opening pressure and opening time increase, and the maximum relative reduction rates are 34.9 and 28.5%, respectively. This demonstrates that the scaled vent size has a relatively small impact on the time interval of external explosion occurrence. Figures 4a, 4b, and 7 show that a greater vented flame propagation speed leads to a shorter corresponding time interval of external explosion occurrence. Therefore, this time interval is directly related to the vented flame propagation speed for different vent parameters. The mechanism accelerating the outdoor vented flame propagation is mainly realised by the turbulence in the unburned gas cloud at the front of the flame [35]. Thus, the outdoor flow field turbulence also produces an indirect effect on the explosion time interval. Simultaneously, the lowest vented flame propagation speed ($v_f = 72.6$ m/s) is reached at $K_v = 0.18$ (see Fig. 4c), but the time interval of explosion occurrence decreases, as shown in Fig. 7. This may be related to the fact that the distribution length of the outdoor high-concentration unburned gas cloud in Fig. 3c is closer to the vent in the axial direction. Thus, the influence of the characteristics of the outdoor unburned gas cloud on the time interval of external explosion occurrence cannot be ignored.

3.2.3. Location of External Explosion Occurrence. The peak combustion rate is plotted in Fig. 8 against the distance for different vent parameters. The location where the maximum peak combustion rate occurs is considered to be the location where the external explosion occurs [21]. It can be seen from Figs. 8a and 8b that, if the opening pressure is lower or the opening time is shorter, the external explosion occurs farther

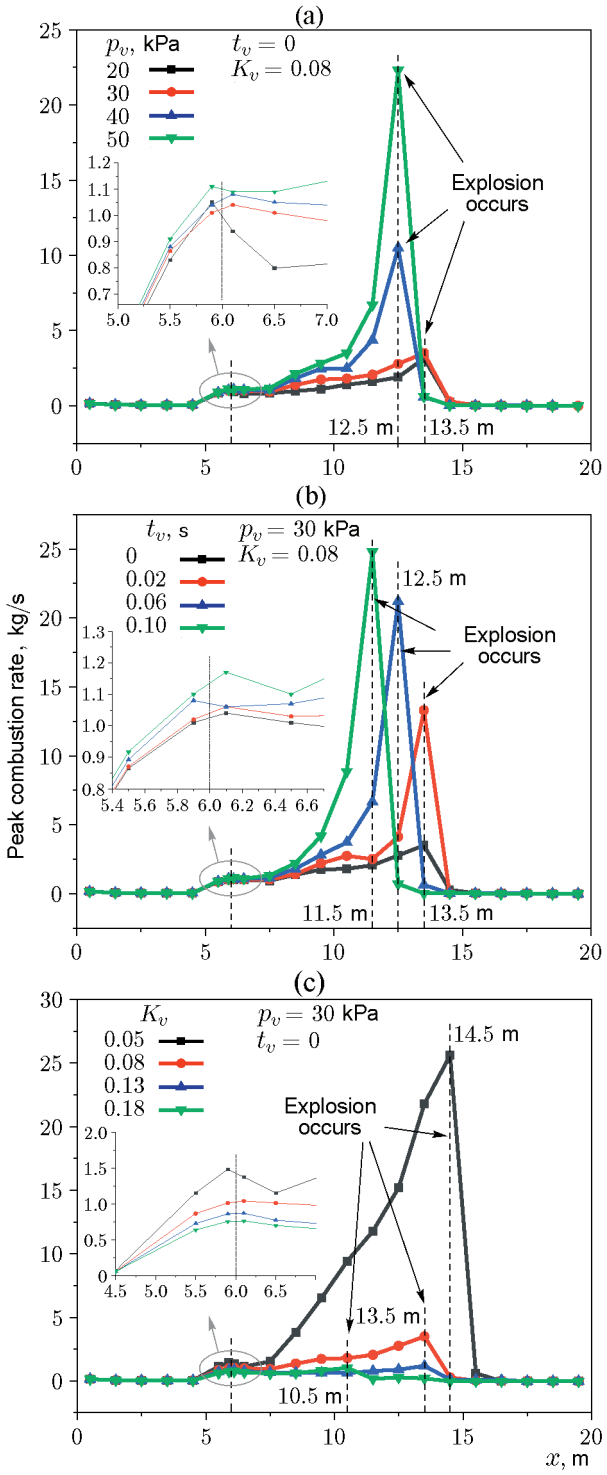

Fig. 8. Peak combustion rate versus the distance for different vent parameters: opening pressure (a), opening time (b), and scaled vent size (c): the insets show the parameters near the vent.

from the vent, reaching a distance of 13.5 m. However, as the vent opening pressure or opening time continues to increase, the vented flame propagation speed near the vent also continuously increases and the distribution length of the high-concentration unburned gas cloud is also closer to the vent in the axial direction at the instant when the outdoor gas cloud is ignited. Thus, the location of the external explosion is closer to the vent, as shown in Figs. 3a and 3b. Figure 8c shows that the external explosion occurs closer to the vent as K_v increases, and the farthest location of the external explosion (14.5 m) is reached at $K_v = 0.05$. This is related to the distribution of the unburned gas cloud outside the vent, as shown in Fig. 3c. Therefore, the distributions of the high-concentration unburned gas cloud parameters exert a significant effect on the location of external explosion occurrence. If the high-concentration unburned gas cloud is located closer to the vent, the external explosion should also occur closer to the vent.

3.3. Correlation between the External Explosion Overpressure and Outdoor Flow Field

As the most intuitive disaster parameter in the study of external explosions, the overpressure has been widely studied by scholars [26]. Figure 9 shows the correlation between the external explosion overpressure (p_e) and flow field parameters, such as the distribution range of the unburned gas cloud (d), flame propagation speed (v_f), and turbulent kinetic energy of the flow field (k) for different vent parameters.

As shown in Fig. 9a, the external explosion overpressure, vented flame propagation speed, and turbulence intensity of the flow field all increase with an increase in the vent opening pressure, while the distribution range of the unburned gas cloud gradually decreases. From Fig. 9b, for the vent opening time $t_v < 0.06$ s, even though the distribution range of the high-concentration unburned gas cloud is large ($d \geqslant 6.3$ m), the flame propagation speed and turbulence intensity of the flow field are relatively small ($v_f \leqslant 93.9$ m/s and $k \leqslant 452$ m^2/s^2), and the overpressure rise caused by the external explosion is still relatively small ($p_e \leqslant 64.5$ kPa). Thus, the external explosion overpressure has a strong positive correlation with the flame propagation speed and flow field turbulence and a negative correlation with the axial distribution range of the unburned gas cloud. However, the opposite correlation is found at $t_v \geqslant 0.06$ s. As the vent opening time increases, a large amount of the gas burns indoors, which reduces the concentration of the unburned gas cloud outdoors, and the outdoor axial distribution of this cloud is shifted toward the vent. Even if the flame propagation speed and flow field turbulence increase, the external explosion overpressure

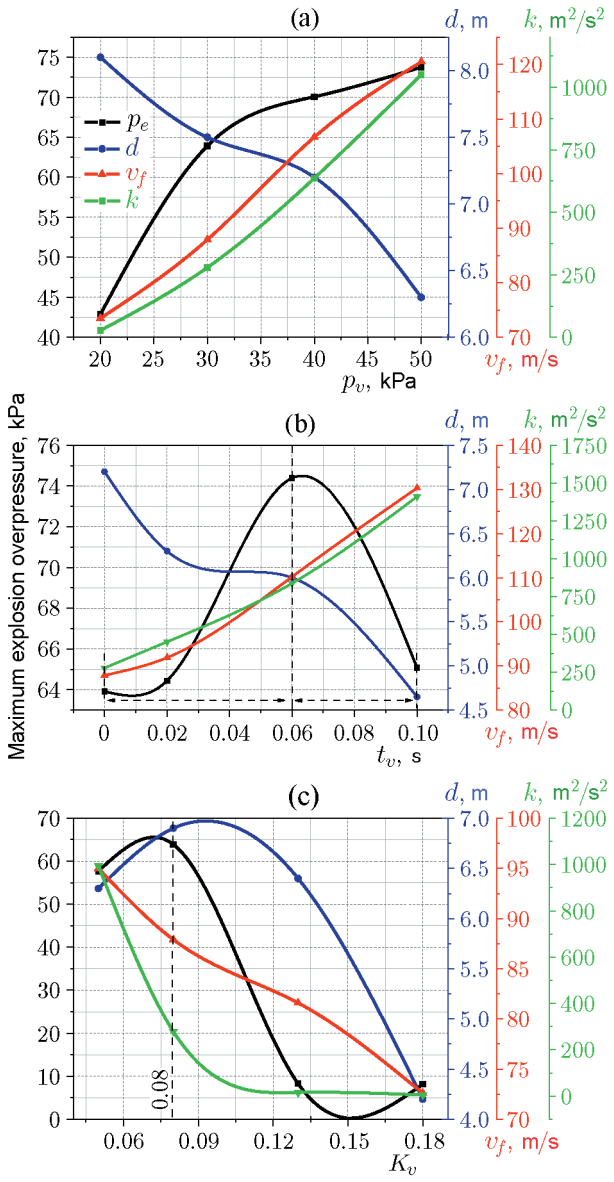

Fig. 9. Correlation between the external explosion overpressure and flow field parameters with variation of the opening pressure (a), opening time (b), and scaled vent size (c).

does not become greater. Meanwhile, Fig. 9c shows that the external explosion overpressure appears to have a strong positive correlation with the distribution range of the unburned gas cloud for different scaled vent sizes because they both maintain the trend of first increasing and then decreasing. At $K_v \geqslant 0.08$, it is found that there is a positive correlation between the external explosion overpressure and the distribution range of the unburned gas cloud, flame propagation speed, and flow field turbulence.

CONCLUSIONS

In this study, a CFD numerical method was used to explore the outdoor flow field characteristics and external explosion distribution laws induced by indoor premixed methane–air explosions with different vent parameters. The main conclusions are formulated as follows.

(1) For a gas explosion in an industrial plant with an explosion-venting surface, the front shape of the outdoor unburned gas cloud and explosion flame change from a jet to a depression in the direction of the vent as the scaled vent size K_v increases from 0.05 to 0.18. The concave shape and axial distribution distance are obviously shortened. The outdoor peak turbulent kinetic energy changes significantly with the vent parameters, up to 1411 m^2/s^2. As the opening pressure p_v increases from 20 to 50 kPa, the axial distance of the outdoor turbulent range reaches 17 m, with an increase of more than two times, which greatly increases the external gas combustion rate and explosion intensity.

(2) For special vent parameters, the external explosion peak overpressure exceeds the indoor overpressure by a factor of more than two. The time interval of external explosion occurrence is significantly shortened as the opening pressure and opening time increase, and the maximum change variation can reach more than 27%; however, the scaled vent size K_v has a minor effect on it. The location of external explosion occurrence is distributed within an area that is approximately 1.4 times the length of the room. At $K_v = 0.05$, the location of external explosion occurrence can reach 14.5 m, indicating that the gas vented explosion process in a larger-scale confined space may produce a wider range of external explosion locations, which will lead to a wider range of vented explosion disaster effects. This should arouse the attention of scholars.

(3) The external explosion overpressure is affected by the external gas cloud distribution, flame jet speed, and outdoor turbulence. At different opening pressures and an opening time of less than 0.06 s, the external explosion overpressure is only positively correlated with the flame propagation speed and outdoor flow field turbulence. As the opening time increases, the external explosion overpressure gradually presents a strong positive correlation with the distribution range of the unburned gas cloud. If the opening time is long, the indoor explosion consumes a large amount of the combustible gas, and the amount of outdoor substances that can participate in the explosion reaction decreases, which ultimately leads to a decrease in the external explosion overpressure. For different scaled vent sizes, the external explosion overpressure always exhibits a strong cor-

relation with the range distribution of the unburned gas cloud. Understanding the present research results will help in developing prevention and control measures to fundamentally reduce the external explosion overpressure and reduce explosion disasters to a certain extent.

The authors appreciate the financial support from the Beijing Natural Science Foundation-Municipal Education Committee Joint Funding Project (Grant No. KZ201910017020), the Training Funded Project of the Beijing Youth Top-Notch Talents of China (Grant No. 20160000026833ZK05), the Science and Technology Plan Project of Beijing Municipal Education Commission (Grant No. KM202010017008), and the Training Funded Project of the Beijing Young Backbone Talents of China (Grant No. 20180000020124G087). At last, we appreciate Elsevier for providing a good English translation service for this manuscript.

REFERENCES

1. F. Q. Yang, J. Guo, C. J. Wang, and S. X. Lu, "Duct-Vented Hydrogen–Air Deflagrations: The Effect of Duct Length and Hydrogen Concentration," Int. J. Hydrogen Energy **43** (45), 21142–21148 (2018); DOI: 10.1016/j.ijhydene.2018.09.074.
2. W. Bartknecht and G. Zwahlen, *Dust Explosions: Course, Prevention, Protection* (Springer-Verlag, Berlin, 1989).
3. Z. H. Chen, B. C. Fan, X. H. Jiang, and J. F. Ye, "Investigations of Secondary Explosions Induced by Venting," Process Saf. Prog. **25** (3), 255–261 (2006); DOI: 10.1002/prs.10139.
4. C. Proust and E. Leprette, "The Dynamics of Vented Gas Explosions," Process Saf. Prog. **29** (3), 231–235 (2010); DOI: 10.1002/prs.10368.
5. O. I. Moen, J. H. S. Lee, B. H. Hjertager, et al., "Pressure Development due to Turbulent Flame Propagation in Large-Scale Methane–Air Explosions," Combust. Flame **47**, 31–52 (1982); DOI: 10.1016/0010-2180(82)90087-6.
6. P. A. Diakow, J. K. Thomas, and E. Vivanco, "Comparison of Large-Scale Vented Deflagration Tests to CFD Simulations for Partially Congested Enclosures," J. Loss Prev. Process Ind. **56**, 147–154 (2018); DOI: 10.1016/j.jlp.2018.07.012.
7. D. P. J. McCann, G. O. Thomas, and D. H. Edwards, "Gasdynamics of Vented Explosions. Part I: Experimental Studies," Combust. Flame **59**, 233–250 (1985); DOI: 10.1016/0010-2180(85)90128-2.
8. M. G. Cooper, M. Fairweather, and J. P. Tite, "On the Mechanisms of Pressure Generation in Vented Explosions," Combust. Flame **65** (1), 1–14 (1986); DOI: 10.1016/0010-2180(85)90128-2.
9. S. K. Chow, R. P. Cleaver, M. Fairweather, and D. G. Walker, "An Experimental Study of Vented Explosions in a 3 : 1 Aspect Ratio Cylindrical Vessel," Process Saf. Environ. Prot. **78** (6), 425–433 (2000); DOI: 10.1205/095758200530970.
10. J. Chao, C. R. Bauwens, and S. B. Dorofeev, "An Analysis of Peak Overpressures in Vented Gaseous Explosions," Proc. Combust. Inst. **33** (2), 2367–2374 (2011); DOI: 10.1016/j.proci.2010.06.144.
11. C. R. Bauwens, J. Chao, and S. B. Dorofeev, "Effect of Hydrogen Concentration on Vented Explosion Overpressures from Lean Hydrogen–Air Deflagrations," Int. J. Hydrogen Energy **37** (22), 17599–17605 (2012); DOI: 10.1016/j.ijhydene.2012.04.053.
12. D. Bradley and A. Mitcheson, "The Venting of Gaseous Explosions in Spherical Vessels. I—Theory," Combust. Flame **32**, 221–236 (1978); DOI: 10.1016/0010-2180(78)90098-6.
13. D. Bradley and A. Mitcheson, "The Venting of Gaseous Explosions in Spherical Vessels. II—Theory and Experiment," Combust. Flame **32**, 237–255 (1978); DOI: 10.1016/0010-2180(78)90099-8.
14. V. V. Molkov, R. Dobashi, M. Suzuki, and T. Hiranob, "Modeling of Vented Hydrogen–Air Deflagrations and Correlations for Vent Sizing," J. Loss Prev. Process Ind. **12**, 147–156 (1999); DOI: 10.1016/S0950-4230(98)00049-7.
15. F. Tamanini, "Scaling Parameters for Vented Gas and Sust Explosions," J. Loss Prev. Process Ind. **14** (6), 455–461 (2001). DOI: 10.1016/S0950-4230(01)00034-1.
16. C. R. Bauwens, J. Chaffee, and S. B. Dorofeev, "Effect of Ignition Location, Vent Size, and Obstacles on Vented Explosion Overpressures in Propane–Air Mixtures," Combust. Sci. Technol. **182** (11/12), 1915–1932 (2010); DOI: 10.1080/00102202.2010.497415.
17. J. Guo, X. X. Sun, S. C. Rui, et al., "Effect of Ignition Location, Vent Size, and Obstacles on Vented Explosion Overpressures in Propane–Air Mixtures," Int. J. Hydrogen Energy **40** (45), 15780–15788 (2015); DOI: 10.1016/j.ijhydene.2015.09.038.
18. J. F. Ye, X. H. Jiang, Z. W. Jia, et al., "Experimental Investigations of External Second-Explosion Induced by Vented Explosion," Explos. Shock Waves **24** (4), 356–362 (2004).
19. Y. Cao, J. Guo, K. L. Hu, et al., "Effect of Ignition Location on External Explosion in Hydrogen–Air Explosion Venting," Int. J. Hydrogen Energy **42** (15), 10547–10554 (2017); DOI: 10.1016/j.ijhydene.2017.01.095.
20. S. H. Zhang and Q. Zhang, "Effect of Vent Size on Vented Hydrogen–Air Explosion," Int. J. Hydrogen

Energy **37** (43), 17788–17799 (2018); DOI: 10.1016/j.ijhydene.2018.07.194.
21. L. Pang, Q. R. Hu, J. J. Zhao, et al., "Numerical Study of the Effects of Vent Opening Time on Hydrogen Explosions," Int. J. Hydrogen Energy **44** (29), 15689–15701 (2019); DOI: 10.1016/j.ijhydene.2019.04.175.
22. S. Sun, M. Y. Wang, Y. Y. Qiu, and K. H. Gao, "Effect of a Hinged Rotating Vent Cover on a Vented Explosion," J. Loss Prev. Process Ind. **57**, 186–193 (2019); DOI: 10.1016/j.jlp.2018.12.002.
23. C. R. Bauwens and S. B. Dorofeev, "Effect of Initial Turbulence on Vented Explosion Overpressures from Lean Hydrogen–Air Deflagrations," Int. J. Hydrogen Energy **39** (35), 20509–20515 (2014); DOI: 10.1016/j.ijhydene.2014.04.118.
24. S. Sun, M. Y. Wang, K. H. Gao, et al., "Effect of Vent Conditions on Internal Overpressure Time-History during a Vented Explosion," J. Loss Prev. Process Ind. **54**, 85–92 (2018); DOI: 10.1016/j.jlp.2018.03.002.
25. A. J. Harrison and J. A. Eyre, "External Explosions as a Result of Explosion Venting," Combust. Sci. Technol. **52**, 91–106 (1987); DOI: 10.1080/00102208708952570.
26. K. Yang, Q. R. Hu, S. H. Sun, et al., "Research Progress on Multi-Overpressure Peak Structures of Vented Gas Explosions in Confined Spaces," J. Loss Prev. Process Ind. **62**, 103969 (2019); DOI: 10.1016/j.jlp.2019.103969.
27. G. Tomlin, D. M. Johnson, P. Cronin, et al., "The Effect of Vent Size and Congestion in Large-Scale Vented Natural Gas/Air Explosions," J. Loss Prev. Process Ind. **35**, 169–181 (2015); DOI: 10.1016/j.jlp.2015.04.014.
28. X. H. Jiang, B. S. Fan, and J. F. Ye, "Turbulence, Vortex and External Explosion Induced by Venting," Appl. Math. Mech. **25** (12), 1390–1397 (2004); DOI: 10.1007/bf02438296.
29. Y. X. Wang, Z. Lian, and Q. Zhang, "Effect of Ignition Location and Vent on Hazards of Indoor Liquefied Petroleum Gas Explosion," Combust. Sci. Technol. **189** (4), 698–716 (2017); DOI: 10.1080/00102202.2016.1246442.
30. Z. M. Du, X. Q. Jin, D. M. Cui, and J. F. Ye, "The Investigation of Correlated Factors of External Explosion during the Venting Process," J. Loss Prev. Process Ind. **19** (4), 326–336 (2006); DOI: 10.1016/j.jlp.2005.07.030.
31. L. Pang, T. Wang, Q. Zhang, et al., "Nonlinear Distribution Characteristics of Flame Regions from Methane–Air Explosions in Coal Tunnels," Process Saf. Environ. Prot. **92** (3), 193–198 (2014); DOI: 10.1016/j.psep.2012.10.016.
32. L. Pang, Q. Zhang, W. Li, et al., "Relationship between Shock Wave and High-Temperature Flow Produced by Gas Explosion in Coal Mine Roadways," Chin. J. High Press. Phys. **25** (5), 457–462 (2011).
33. H. Zhang, Y. B. Li, J. J. Xiao, and T. Jordan, "Large Eddy Simulations of the All-Speed Turbulent Jet Flow Using 3-D CFD Code GASFLOW-MPI," Nucl. Eng. Des. **328**, 134–144 (2018); DOI: 10.1016/j.nucengdes.2017.12.032.
34. S. V. Patankar, *Numerical Heat Transfer and Fluid Flow* (Hemisphere, Washington, DC, 1980).
35. E. Salzano, F. S. Marra, G. Russo, and J. H. S. Lee, "Numerical Simulation of Turbulent Gas Flames in Tubes," J. Hazard. Mater. **95** (3), 233–247 (2002); DOI: 10.1016/S0304-3894(02)00161-9.
36. B. E. Launder and D. B. Spalding, *Mathematical Models of Turbulence* (Academic Press, London, 1972).
37. K. N. C. Bray, "Studies of the Turbulent Burning Velocity," Proc. Roy. Soc. London A **431**, 315–325 (1990); DOI: 10.1098/rspa.1990.0133.